Angiogenesis (2018) 21:363–380
https://doi.org/10.1007/s10456-018-9602-0

ORIGINAL PAPER

Vascular deficiency of *Smad4* causes arteriovenous malformations: a mouse model of Hereditary Hemorrhagic Telangiectasia

Angela M. Crist[1] · Amanda R. Lee[1] · Nehal R. Patel[1] · Dawn E. Westhoff[1] · Stryder M. Meadows[1]

Received: 18 October 2017 / Accepted: 28 January 2018 / Published online: 19 February 2018

Abstract

Hereditary hemorrhagic telangiectasia (HHT) is an autosomal dominant vascular disorder that leads to abnormal connections between arteries and veins termed arteriovenous malformations (AVM). Mutations in TGFβ pathway members *ALK1*, *ENG* and *SMAD4* lead to HHT. However, a *Smad4* mouse model of HHT does not currently exist. We aimed to create and characterize a *Smad4* endothelial cell (EC)-specific, inducible knockout mouse (*Smad4*$^{f/f}$;*Cdh5*-Cre^{ERT2}) that could be used to study AVM development in HHT. We found that postnatal ablation of *Smad4* caused various vascular defects, including the formation of distinct AVMs in the neonate retina. Our analyses demonstrated that increased EC proliferation and size, altered mural cell coverage and distorted artery–vein gene expression are associated with *Smad4* deficiency in the vasculature. Furthermore, we show that depletion of *Smad4* leads to decreased *Vegfr2* expression, and concurrent loss of endothelial *Smad4* and *Vegfr2* in vivo leads to AVM enlargement. Our work provides a new model in which to study HHT-associated phenotypes and links the TGFβ and VEGF signaling pathways in AVM pathogenesis.

Keywords Smad4 · Arteriovenous malformations (AVM) · Hereditary hemorrhagic telangiectasia (HHT) · Vegfr2 · TGFβ

Introduction

Hereditary hemorrhagic telangiectasia (HHT) is an autosomal dominant vascular disorder that affects 1 in 5000 people worldwide [1, 2]. HHT patients commonly exhibit: spontaneous, recurring nosebleeds; small lesions on mucous membranes called telangiectasias; and/or larger visceral lesions known as arteriovenous malformations (AVMs) [3, 4]. AVMs, which are direct connections between arteries and veins, are most commonly found in major organs such as the brain, liver or lungs. These lesions present a serious health risk and can lead to decreased quality of life and/or early death due to hemorrhaging, stroke and aneurysms [3, 5–8].

Approximately 85% of HHT cases are linked to heterozygous loss-of-function mutations in the transforming growth factor beta (TGFβ) cell surface receptors activin receptor-like kinase 1 (*ALK1*, HHT2) or endoglin (*ENG*, HHT1) [9, 10]. A small subset of HHT patients (~ 4%) exhibit haploinsufficiency of Mothers against decapentaplegic homolog 4 (*SMAD4*, JP/HHT) and commonly present with juvenile polyposis syndrome (JP) [11, 12]. SMAD4 is a transcription factor found in nearly all cell types [13, 14], where it serves as the central conduit through which canonical TGFβ signaling proceeds, including ALK1 and ENG signaling [15]. However, despite the key role of SMAD4 in the TGFβ pathway, the mechanisms by which it contributes to HHT pathogenesis remain unknown. In fact, virtually all HHT animal studies have focused on the *Alk1* and *Eng* receptor interface of the TGFβ signaling pathway, whereby endothelial loss of *Alk1*, or *Eng* or blockade of the TGFβ pathway via *Bmp9/10* ligand-blocking antibodies results in HHT-associated phenotypes [16–26]. What little we know about the in vivo role of SMAD4 in the vasculature comes from embryonic studies. These studies revealed that SMAD4 plays a critical role in blood vessel remodeling and maturation [27], integrity of the blood-brain barrier endothelium [28] and regulating coronary artery size [29]. Conversely, nothing is known about SMAD4 function in the postnatal vasculature as homozygous loss of *Smad4* is embryonic lethal [27]. Therefore, due

Electronic supplementary material The online version of this article (https://doi.org/10.1007/s10456-018-9602-0) contains supplementary material, which is available to authorized users.

✉ Stryder M. Meadows
smeadows@tulane.edu

[1] Cell and Molecular Biology Department, Tulane University, New Orleans, LA 70118, USA

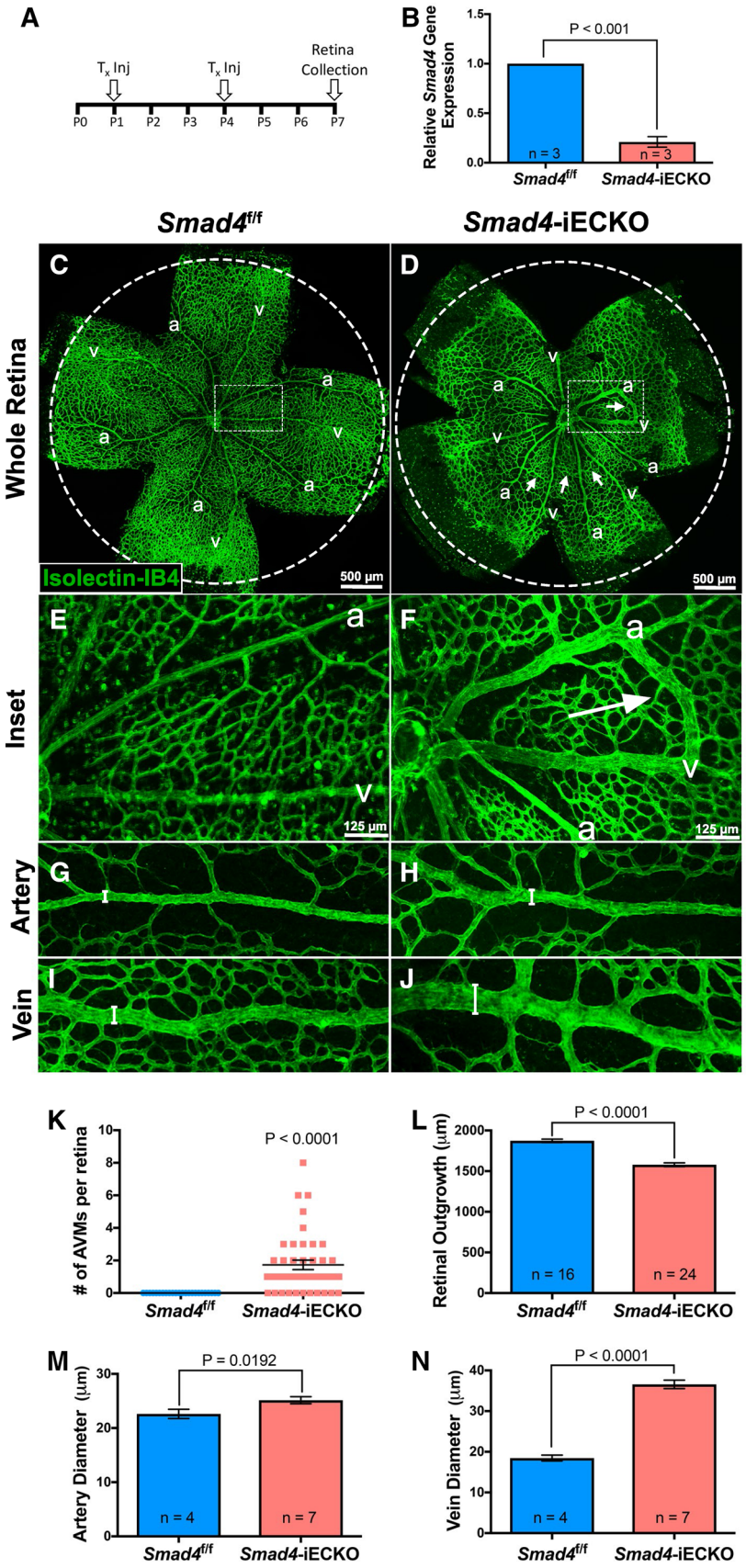
A
Tx Inj
Tx Inj
Retina Collection
P0 P1 P2 P3 P4 P5 P6 P7
B
Relative Smad4 Gene Expression
P < 0.001
n = 3
n = 3
Smad4f/f
Smad4-iECKO
Smad4f/f
Smad4-iECKO
Whole Retina
Inset
Artery
Vein
C
D
Isolectin-IB4
500 μm
500 μm
E
F
125 μm
125 μm
G
H
I
J
K
# of AVMs per retina
P < 0.0001
Smad4f/f
Smad4-iECKO
L
Retinal Outgrowth (μm)
P < 0.0001
n = 16
n = 24
Smad4f/f
Smad4-iECKO
M
Artery Diameter (μm)
P = 0.0192
n = 4
n = 7
Smad4f/f
Smad4-iECKO
N
Vein Diameter (μm)
P < 0.0001
n = 4
n = 7
Smad4f/f
Smad4-iECKO

◂**Fig. 1** Multiple vascular defects, including AVMs, are associated with endothelial loss of *Smad4*. **A** Schematic outlining tamoxifen (Tx) injections in *Smad4*$^{f/f}$ (control) and *Smad4*$^{f/f}$;*Cdh5*-Cre^{ERT2} (hereafter referred to as *Smad4*-iECKO) neonate pups. **B** qPCR using RNA from freshly isolated retinal endothelial cells shows an 80% reduction in *Smad4* transcript levels (normalized to *Cd31*). **C–J** Confocal images of *Smad4*$^{f/f}$ and *Smad4*-iECKO P7 retinas stained with isolectin-IB4 (IB4, green) to mark the retinal vasculature. **C**, **D** *Smad4*$^{f/f}$ and *Smad4*-iECKO whole retina images illustrate the presence of AVMs (arrows) and reduced vascular outgrowth in *Smad4*-deficient genetic backgrounds. Dotted circles represent outgrowth of the control retina. Scale bar: 500 µm. **E**, **F** Magnified images of dotted boxes in **C** and **D** show normal separation of arteries and veins in control retinas, while *Smad4* mutants contained obvious AVMs (arrow). Scale bar: 125 µm. **G**, **H** Close-up views of a *Smad4*$^{f/f}$ artery versus a *Smad4*-iECKO artery. Note the increased diameter of *Smad4* mutant arteries. **I**, **J** Close-up views of a *Smad4*$^{f/f}$ vein versus a *Smad4*-iECKO vein. Note the increased diameter of *Smad4* mutant veins. **K** Quantification of the number of AVMs per retina in *Smad4* control and mutant backgrounds. **L** *Smad4*-iECKO mutants exhibited reduced vascular outgrowth toward the retinal periphery. Outgrowth was measured by taking the distance from the optic nerve to the outermost vessel in the vascular front. Four measurements were taken per retina (one on each retinal leaflet). **M**, **N** Graphs showing increased artery (**M**) and vein (**N**) diameters in *Smad4*-iECKO retinas compared to *Smad4*$^{f/f}$ controls. Three points were measured on each vessel type (proximal, medial and distal from the optic nerve), and three arteries and veins were randomly chosen and measured per retina. *a* arteries, *v* veins. All Fig. 1 statistics include *Smad4* mutant retinas with and without AVMs, and areas around and separate from AVMs

to limited information on how SMAD4 contributes to the developing endothelium, it is unclear how SMAD4 defects lead to HHT phenotypes, such as AVM formation.

In order to better understand SMAD4's contribution to HHT pathogenesis, we created an inducible, endothelial cell (EC)-specific *Smad4* knockout mouse model (referred to as *Smad4*-iECKO). We find that induced deletion of *Smad4* leads to various vascular defects including the formation of AVMs. In addition, we show that SMAD4 influences EC proliferation, EC size, mural cell coverage and artery–vein gene expression. Utilizing this new *Smad4*-iECKO model, we found that deletion of *Smad4* leads to decreased levels of vascular endothelial growth factor receptor 2 (VEGFR2) expression. Furthermore, concurrent loss of endothelial *Smad4* and *Vegfr2* in vivo leads to an increased AVM severity. This work provides a new model for the HHT field and presents evidence that the TGFβ and VEGF pathways may be linked in AVM pathogenesis.

Results

EC-specific deletion of *Smad4* causes multiple vascular defects, including AVM formation

To characterize SMAD4 function in the postnatal vasculature, *Cdh5*-Cre^{ERT2} [30] and conditional *Smad4*-floxed (Smad4$^{f/f}$) [31] mouse lines were utilized to generate homozygous *Smad4*-inducible, endothelial-specific knockout mice (*Smad4*-iECKO). Tamoxifen (Tx) injections were administered at postnatal day 1 (P1) and P4 to activate Cre-mediated deletion of *Smad4* in the endothelium (Fig. 1A). A majority of mice died around P8–P9, likely due to respiratory distress caused by defects in the lung vasculature (Fig. S1A–B′), similar to *Alk1*-deficient neonate mice [20]. Therefore, we utilized P7 retinas to assess blood vessel development, as the retina is a tractable system for identifying vascular defects, including AVMs, and has been used to study *Alk1* and *Eng* mouse models of HHT.

To confirm *Smad4* deletion in the endothelial lineage, quantitative PCR (qPCR) was performed using RNA from P7 *Smad4*$^{f/f}$ (control) and *Smad4*-iECKO isolated retinal ECs which revealed an ~ 80% reduction in *Smad4* mRNA transcripts (Fig. 1B). In addition, using a *Rosa26*-EYFP transgenic reporter line [32] we confirmed that Cre-recombinase was specifically expressed in blood vessels, while absent in control blood vessels (Fig. S1C–D′). These data demonstrated efficient and specific *Smad4* knockdown in the ECs of *Smad4*-iECKO retinas.

In order to assess the effects of *Smad4* depletion on vascular development, *Smad4*$^{f/f}$ control and *Smad4*-iECKO P7 retinas were labeled with the vascular marker Isolectin-IB4. We observed numerous arteriovenous malformations (AVMs) in the retinas of *Smad4* mutants (Fig. 1C–F), similar to those identified in *Alk1*- and *Eng*-deficient mice [17, 18, 20, 24, 33, 34]. Approximately 82% of our *Smad4* mutants had AVMs, whereas AVMs were absent in all controls. Multiple AVMs were seen in 52% of *Smad4*-iECKO mice with an average of 1.732 AVMs per mutant retina (Fig. 1K). AVMs varied in morphology but were easily identifiable because the shunts appeared grossly enlarged in comparison with normal capillaries (Fig. 1C–F and Fig. S2A–H). AVMs were almost always located near the center of the retina, likely due to blood flow patterns in HHT models as previously described [35]. In *Smad4*-iECKO mice, AVMs form around P5 (data not shown) and either did not form or were smaller if Tx was administered after P1 (Fig. S2I–K).

Loss of *Smad4* also caused a noticeable reduction in vascular outgrowth toward the retinal periphery (Fig. 1C, D, L). For this reason and because *Alk1* mutant zebrafish exhibit EC migratory defects [36], we aimed to further assess *Smad4* function on EC migration in vitro. We generated

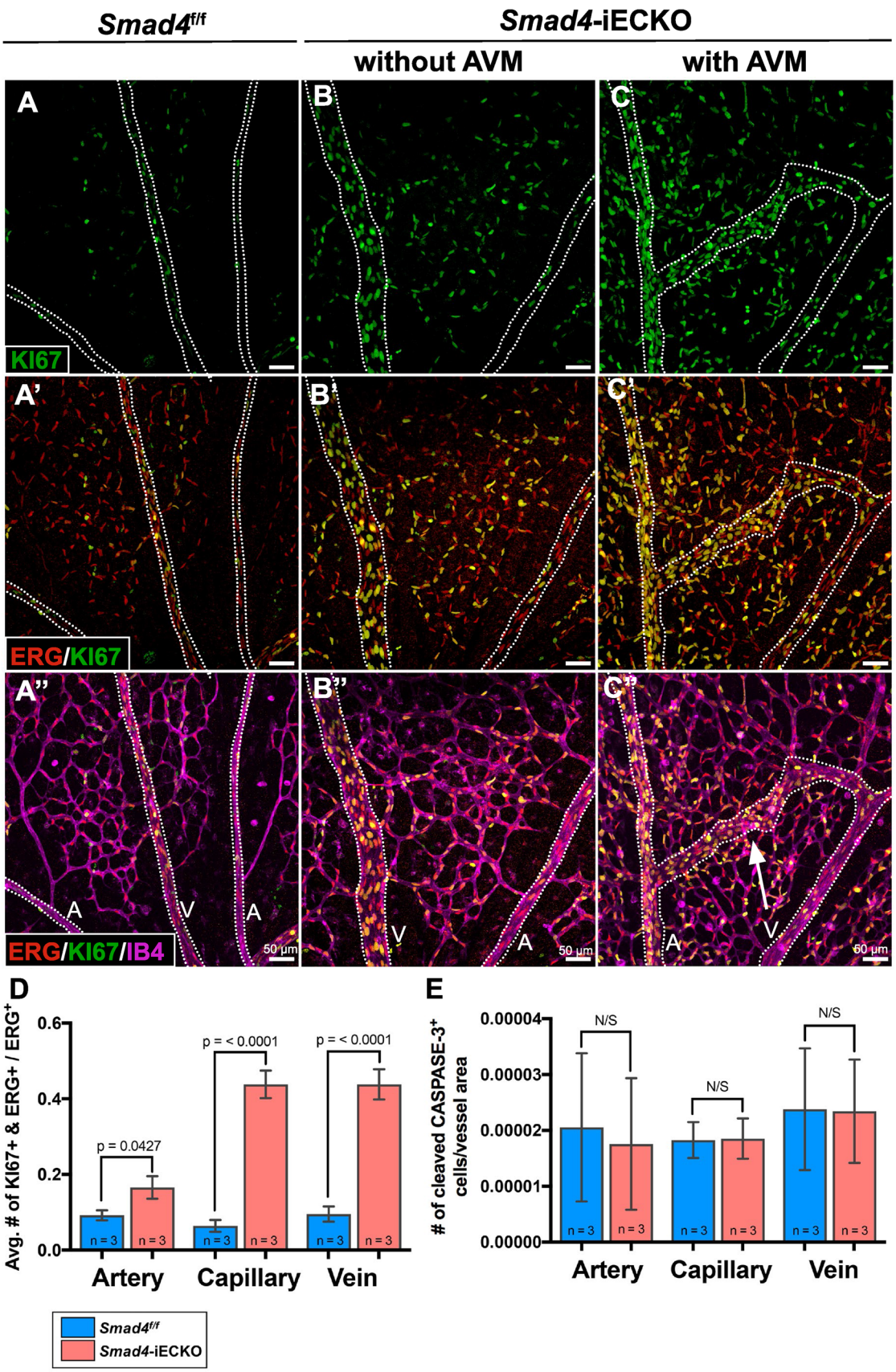
Smad4f/f
Smad4-iECKO
without AVM
with AVM
A
B
C
KI67
A'
B'
C'
ERG/KI67
A''
B''
C''
A
V
A
ERG/KI67/IB4
50 µm
V
A
50 µm
A
V
60 µm
D
Avg. # of KI67+ & ERG+ / ERG+
0.6
0.4
0.2
0.0
p = 0.0427
p = < 0.0001
p = < 0.0001
n = 3
Artery
Capillary
Vein
Smad4f/f
Smad4-iECKO
E
# of cleaved CASPASE-3+ cells/vessel area
0.00004
0.00003
0.00002
0.00001
0.00000
N/S
N/S
N/S
n = 3
Artery
Capillary
Vein

◂**Fig. 2** Increased cell proliferation in *Smad4*-deficient ECs. **A**–**C**" Close-up views of $Smad4^{f/f}$ and *Smad4*-iECKO P7 retina stained for KI67 (green), ERG (red) and Isolectin-IB4 (magenta; IB4). *a* arteries, *v* veins and AVM (white arrow) in **A**–**C**' are outlined by dotted lines. Scale bars = 50 µm. **D** *Smad4* deficiency leads to an increase in proliferating ECs ($KI67^+$ and ERG^+) in *Smad4*-iECKO arteries, capillaries and veins. Three fields of view were counted in each sample. **E** Loss of *Smad4* reveals no change in the number of apoptotic cells as assessed by cleaved CASPASE-3 fluorescence in the P7 retinal vasculature. Three fields of view were counted in each sample. Sample size (*n*) indicates independent biological samples

stable C166 mouse EC lines that expressed either nonsilencing-shRNAs or Smad4-shRNAs. In comparison with nonsilencing-shRNA, Smad4-shRNA C166 cells showed an approximately 60% reduction in levels of *Smad4* transcripts and a diminished capacity to migrate and repopulate wounds in a scratch assay (Fig. S3A–D).

Although outgrowth was stunted, the number of tip cells was not significantly changed in *Smad4* mutant retinas (data not shown). Similarly, quantification of vascular densities showed no statistical differences on average (data not shown). This is likely due to the high variability between mutants, as we observed some mutants that displayed significant increases in density in the tip region, while others were indistinguishable from controls (Fig. S4). Although there was variability among vascular density of mutants, one consistent phenotype was that of increased artery and vein diameters (Fig. 1G–J, M, N). Increases in vessel diameter and stunted outgrowth were also even seen in the ~ 20% of mutants that did not express AVMs, suggesting that these events may precede AVM development.

Collectively, these results demonstrate that *Smad4* is required for proper vascular growth and vessel morphology in the postnatal retina. Furthermore, the presence of AVMs verifies that loss of *Smad4* in mice recapitulates phenotypes associated with HHT patients, thus making this a suitable model for studying *Smad4* mechanisms of HHT.

Smad4 depletion causes increases in EC proliferation and size

To determine whether vessel enlargement was caused by an increase in EC proliferation, we examined both *Smad4* control and mutant retinas immunolabeled for the proliferation-associated protein, KI67, and the EC-specific nuclear marker, ERG. Proliferating ECs, which are defined as both KI67 and ERG positive, were quantified in the arteries, veins and capillaries (Fig. 2A–D). We found significant increases in proliferation in all vessel types, with the most drastic changes seen in the capillaries and veins. Increases in proliferation occurred in vascular regions with and without AVMs, indicating that these increases are attributable to reduction in SMAD4 levels and not an effect of AVM formation itself. Conversely, staining for the apoptotic marker cleaved CASPASE-3 revealed no changes in cells undergoing apoptosis between control and *Smad4*-iECKO retinal blood vessels (Fig. 2E). These data indicated that increased rates of EC proliferation, at least in part, are responsible for the increased vessel sizes in *Smad4*-iECKO retinas.

Relatedly, recent reports indicated that loss of either *Eng* or *Smad4* leads to an increased EC size [25, 29], which could contribute to an increased artery and vein diameter and/or AVM formation. To determine whether *Smad4*-iECKO mice exhibited changes in cell size, we measured EC areas in each vessel type as marked by CD31-stained EC boundaries. *Smad4* deletion caused the cell area of arterial ECs to increase by 41%, while venous ECs increased by 34% compared to their respective control vessels (Fig. 3A–F). In addition, C166 ECs with Smad4-shRNA showed a 115% increase in cell area compared to nonsilencing-shRNA C166 ECs (Fig. 3G–I). Overall, these results are consistent with a recent study showing that loss of *Smad4* contributes to an increase in cell size in the developing coronary artery and in cultured ECs under high levels of shear stress [29]. Taken together, we conclude that a combination of an increased EC proliferation and an increased EC size contributes to the vessel enlargement phenotypes observed in *Smad4* mutants.

Defective mural cell coverage in *Smad4*-iECKO mice

Alk1 and *Eng* models of HHT have previously noted several changes in mural cell coverage of retinal blood vessels. For instance, vascular smooth muscle cells (vSMCs) were found to accumulate ectopically around veins [17, 20, 24]. In *Smad4*-iECKO mice, we also observed strong, ectopic expression of alpha-smooth muscle actin (αSMA) protein around the AVMs and veins compared to control retinas which only exhibit αSMA on arteries at P7 (Fig. 4A–B'). Moreover, qPCR analysis demonstrated increased *αSma* transcript levels in *Smad4*-iECKO retinas compared to $Smad4^{f/f}$ controls (Fig. 4C).

Conversely, AVMs are associated with a reduction in pericyte coverage [20, 35]. *Smad4* deficiency has been shown to affect EC–pericyte interactions resulting in loss of pericyte coverage in the developing brain vasculature [28]. To test whether this relationship exists in *Smad4*-iECKO retinas, we investigated pericyte coverage using an anti-neuron-glial antigen 2 (NG2) antibody. We found that compared to controls, *Smad4* mutant retinas exhibit a marked reduction in NG2 protein accumulation in the retinal vasculature (Fig. 4D–E'). Furthermore, qPCR analysis on whole retina samples verified that *Ng2* and *Desmin* (a pericyte marker) mRNA levels are significantly diminished when *Smad4* is deleted (Fig. 4F, G). Since the platelet-derived growth factor (PDGF) signaling pathway plays a significant role

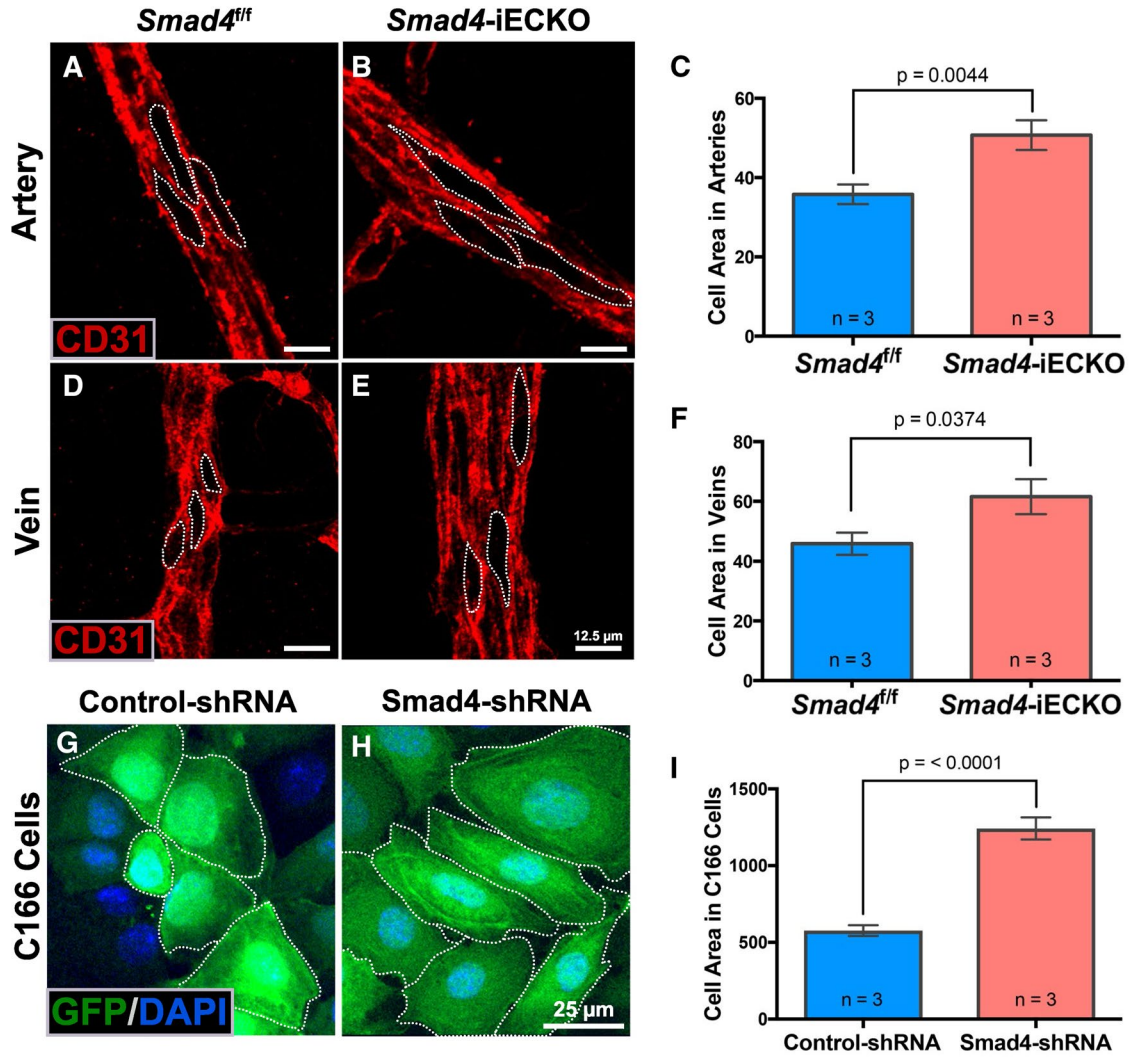

Fig. 3 Loss of *Smad4* causes an increased EC size. **A**–**E** *Smad4*$^{f/f}$ and *Smad4*-iECKO P7 retinal arteries (**A**, **B**) and veins (**D**, **E**) immunolabeled for CD31/PECAM (red) to mark EC–EC boundaries revealed an increase in cell size upon loss of *Smad4*. Scale bar: 12.5 µm. **C**, **F** Quantification of EC areas within CD31-stained regions demonstrated enlarged ECs in both arteries and veins of *Smad4* mutants compared to controls. Sample size (*n*) indicates independent animals. Three ECs from each of three random arteries and veins were measured per retina. For these experiments, we did not categorize vessels as near or far from AVMs, and mutants with and without AVMs were included. **G**–**H** GFP- and DAPI-stained nonsilencing-shRNA and Smad4-shRNA C166 cells expressing an internal ribosome entry site (IRES) mediated GFP. Dotted lines mark the cell boundaries as distinguished by the cytoplasmic GFP. Scale bar: 25 µm. **I** Quantification of EC sizes showed significant increases in cell areas of Smad4-shRNA cells compared nonsilencing-shRNA C166 cells. For image quantification, three fields of view were used per sample and a minimum of three ECs was measured per field of view

in recruiting pericytes to blood vessels [37], we assessed whether changes in expression of the endothelial-secreted PDGFB ligand could account for the loss of pericyte coverage in *Smad4* mutants. qPCR results showed that *Pdgfb* transcript levels are similar in control and *Smad4*-iECKO whole retinas (Fig. 4H), suggesting that other factors are responsible for the reduced pericyte presence in *Smad4*-deficient retinas. Overall, our results are consistent with other HHT models in that vSMC coverage inappropriately extends to AVMs and veins, while pericyte coverage is reduced in a *Smad4*-deficient background.

Artery–vein identity is disrupted in the absence of *Smad4*

The presence of vSMCs on *Smad4*-deficient veins suggested that these vessels may have acquired an arterial-like identity. Interestingly, alterations in artery and vein (AV) gene expression have been reported in HHT models [17, 20, 38, 39] and in non-HHT-associated AVMs triggered by disruptions in NOTCH pathway signaling components [40, 41]. Therefore, we characterized a number of AV identifiers, including NOTCH pathway members, in our *Smad4*-iECKO

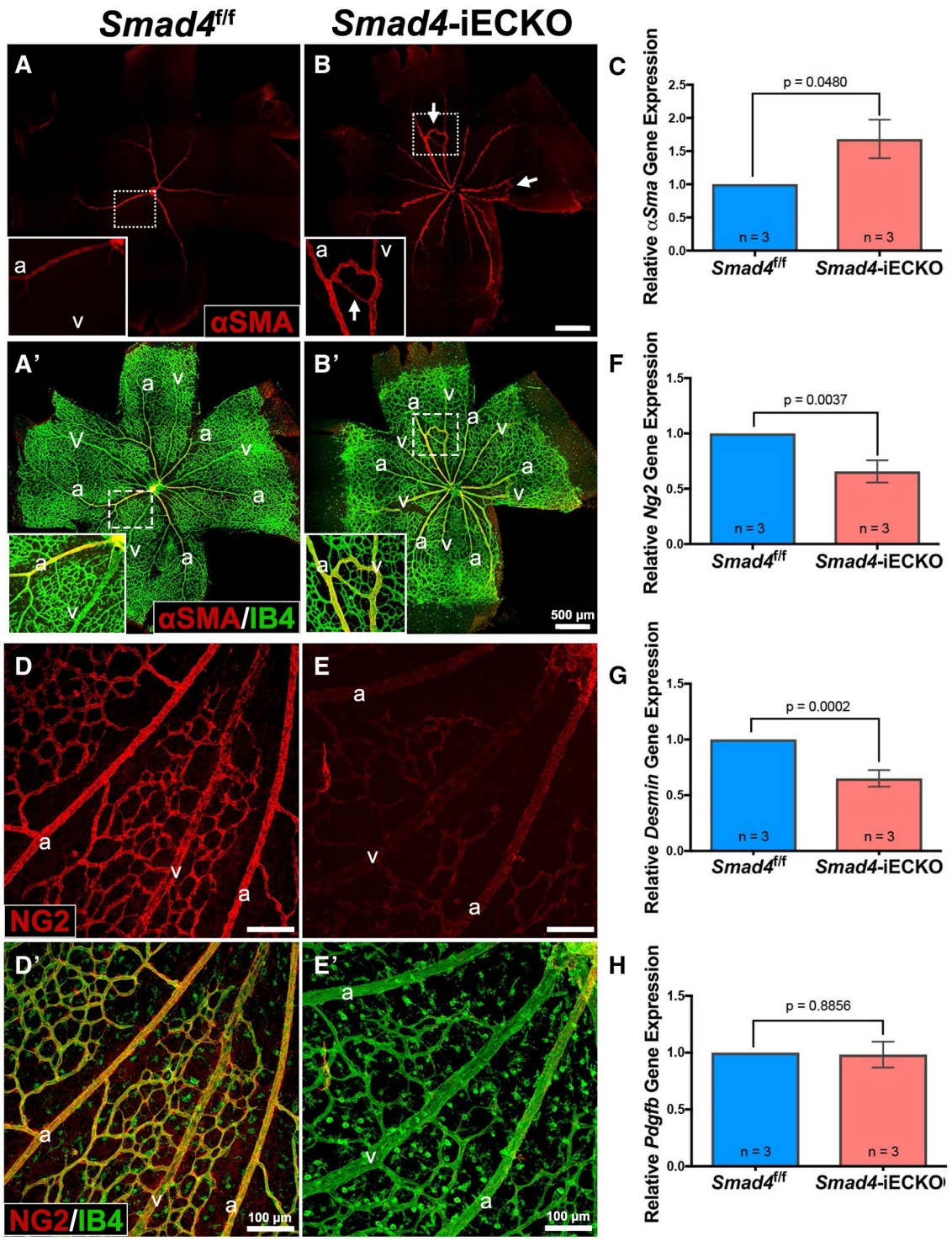

Fig. 4 Altered mural cell coverage in *Smad4*-iECKO retinas. **A**–**B**' Confocal analysis of alpha-smooth muscle actin (αSMA; red) and Isolectin-IB4 (IB4; green) revealed that *Smad4*$^{f/f}$ retinas (n = 10) contain αSMA only on arteries, whereas *Smad4*-iECKO mice (n = 8) express αSMA on both arteries and veins. Insets show close-up views of an artery and vein, with an AVM covered by αSMA in **B**, **B′** inset. AVMs are denoted by white arrows in **B**. **C** qPCR results on RNA isolated from *Smad4*$^{f/f}$ and *Smad4*-iECKO P7 whole retinas confirm an increased *αSma* gene expression in Smad4 mutants. **D**–**E**' Immunofluorescent staining of the pericyte marker neuron-glial antigen 2 (NG2; red) and IB4 (green) revealed a striking reduction in levels of NG2 in *Smad4*-iECKO mice (n = 9) compared to control (n = 10). **F**, **G** qPCR analysis of *Ng2* and *Desmin* (another pericyte marker) transcript levels in P7 *Smad4*$^{f/f}$ and *Smad4*-iECKO whole retinas verifies loss of pericytes in *Smad4*-deficient backgrounds. **H** qPCR analysis of secreted ligand *Pdgfb* transcript levels in P7 *Smad4*$^{f/f}$ and *Smad4*-iECKO whole retinas remains unchanged. *a* arteries, *v* veins. The number of independent biological samples is shown as (*n*) on bar graphs, and all qPCR samples were normalized to the housekeeping gene *Odc*

model by performing qPCR on isolated lung endothelial cells (iLECs) from *Smad4* mutants and their control littermates (Fig. 5A). We found a significant reduction in the venous-associated markers *CouptfII* and *Ephb4* and arterial markers *Hey1, Hey2, Notch1* and *Nrp1*. Conversely, mRNA levels of the venous markers, *Endomucin* and *Flt4*, and the arterial markers *Apelin* (also associated with vascular tip cells) and *Notch4* were upregulated in *Smad4*-iECKO iLECs. The following markers remained unchanged between *Smad4* control and mutants: *Apj, Cx40, Dll4, Ephrinb2, Jagged1, Nrp2* and *Sox17*.

To further confirm changes in AV gene expression, we used immunofluorescent staining and in situ hybridization techniques on *Smad4*$^{f/f}$ and *Smad4*-iECKO retinas. At P7, ENDOMUCIN is largely absent from control retinal arteries (Fig. 5B); however, in *Smad4* mutants, we observed distinct protein expression in the arteries (Fig. 5C), suggesting that increased *Endomucin* mRNA levels in iLECs (Fig. 5A) might be due to enhanced expression in arteries. Analysis of *Apelin* mRNA showed robust, ectopic expression in the retinal veins and capillaries of *Smad4* mutants compared to controls, which completely lacked expression in these vessels (Fig. 5D, E). On the other hand, the apelin receptor, *Apj*, was present in the AVM but showed no noticeable changes in mRNA expression between *Smad4* control and mutant retinas consistent with our qPCR results (Fig. 5F, G). Examination of *Ephb4* revealed the loss of transcripts in the capillaries and arteries, although *Ephb4* mRNA remained in the veins (Fig. 5H, I). Interestingly, even though overall levels of *Ephb4* mRNA were reduced, *Ephb4* was still noticeably expressed within the AVM and the artery connected in the AVM. Analysis of *Notch4* showed no changes in localization of transcripts between *Smad4* control and mutant retinas; however, levels of *Notch4* appeared markedly higher in *Smad4*-iECKO retinas (Fig. 5J, K). In all, the whole retina staining results are consistent with the qPCR analysis performed on iLECs. This also revealed the importance of examining both qPCR levels in the whole vasculature as well as localization changes, as some markers are gained in specific vascular beds (*Apelin*), while others are lost (*Ephb4*). More so, some markers can increase in levels without changing localization (*Notch4*), while others remain the same but are expressed in the AVM (*Apj*). Therefore, we conclude that loss of *Smad4* in the endothelium alters AV gene expression and as other groups have suggested may play a contributing role in the formation of AVMs due to disruptions in vessel identity [41].

In addition, we quantified the transcript levels of *Alk1* and *Eng* in *Smad4* control and mutant iLECs, as previous reports have shown that genetic knockdown of one receptor can lead to changes in expression of the other in vivo [17, 20, 24]. Our qPCR results indicate a significant loss in expression of *Eng* in *Smad4*-depleted ECs; however, no changes in *Alk1* expression were observed (Fig. 5A).

Loss of *Vegfr2* enhances *Smad4* mutant phenotypes

Recent investigations in *Alk1* and *Eng* HHT models indicated a potential link with vascular endothelial growth factor receptor 2 (*Vegfr2*) [24, 34, 42], a major signaling component in the VEGF pathway. In order to determine whether *Smad4* and *Vegfr2* are associated in AVM pathogenesis, we first assessed whether *Vegfr2* mRNA levels were altered in our *Smad4*-iECKO background. qPCR analysis on cultured iLECs demonstrated that, in comparison with controls, *Vegfr2* mRNA levels are reduced by approximately 40% in *Smad4*-iECKO mice (Fig. 6A). However, no significant changes in *Vegfr2* transcript levels were observed between Tx-injected *Smad4*$^{f/f}$ control and *Smad4*$^{f/+}$;*Cdh5*-Cre^{ERT2} iLECs, even though *Smad4* mRNA levels were reduced by approximately 50% in the heterozygous mutants (data not shown). Similarly, quantification in Smad4-shRNA C166 endothelial cells also showed a relationship whereby *Vegfr2* transcripts were significantly reduced compared to nonsilencing-shRNA controls (Fig. 6B). Moreover, expression of VEGFR2 protein was dramatically diminished in *Smad4*-deficient iLECs (Fig. 6C, D) and appeared reduced throughout all retinal blood vessels in *Smad4* mutants as compared to controls (Fig. 6E–H). In all, these data demonstrated that impaired SMAD4 function leads to significantly reduced expression of *Vegfr2* mRNA and protein.

Since our data indicated that *Vegfr2* expression decreases upon loss of *Smad4*, we hypothesized that the incremental losses of VEGFR2 in the *Smad4*-iECKO background would lead to enhanced HHT-like phenotypes during retinal vascular development. To test this possibility, we crossed our *Smad4*-iECKO mouse line to *Vegfr2*-floxed mice (*Vegfr2*$^{f/f}$, referred to as *Vegfr2*$^{f/+}$-iECKO or *Vegfr2*$^{f/f}$-iECKO in the presence of *Cdh5*-Cre^{ERT2}) [43]. The different genetic combinations of mice were given Tx at P1, and retinas were collected at P7. Similar to control *Smad4*$^{f/f}$ mice lacking *Cdh5*-Cre^{ERT2}, a single allelic deletion of *Smad4* (*Smad4*$^{f/+}$-iECKO) had no noticeable effects on retinal vascular development, while *Vegfr2* (*Vegfr2*$^{f/+}$-iECKO) retinas only showed a reduction in vascular outgrowth (Fig. 7A, B, D). On the other hand, the combined loss of a single allele of *Smad4* and *Vegfr2* (*Smad4*$^{f/+}$;*Vegfr2*$^{f/+}$-iECKO) resulted in increases in vascular density at the growing front (although inconsistent), which were never observed in *Smad4*$^{f/+}$-iECKO or *Vegfr2*$^{f/+}$-iECKO retinas, but were similar to *Smad4*$^{f/f}$-iECKO retinas (compare Fig. 7 B–E and Fig. S4). More compellingly, loss of a single copy of the *Vegfr2* allele in the *Smad4*-iECKO background (*Smad4*$^{f/f}$;*Vegfr2*$^{f/+}$-iECKO) revealed dramatic vascular

phenotypes beyond those observed in *Smad4*-iECKO mice alone (compare Fig. 7C and F). Vascular outgrowth was significantly inhibited, and the vascular front showed reliable and marked increases in density (Fig. 7J). Even more noticeable was the increased number and striking enlargement of AVMs. We quantified severity of AVMs by measuring the diameter of the AVM in *Smad4*-iECKO and *Smad4*$^{f/f}$;*Vegfr2*$^{f/+}$-iECKO mice. On average, *Smad4*$^{f/f}$;*Vegfr2*$^{f/+}$-iECKO AVMs were ~ 75 µm wider than *Smad4*-iECKO AVMs, suggesting that more blood is able to be shunted from artery to vein in these AVMs leading to a more severe phenotype (Fig. 7K–M). Together, these experiments implied that overall levels of VEGFR2 have an effect on severity of *Smad4*-mediated HHT phenotypes.

Interestingly, reciprocal experiments in *Vegfr2* null backgrounds showed slightly different results. As previously observed, complete loss of *Vegfr2* (*Vegfr2*$^{f/f}$-iECKO) in the retina led to severe vascular defects, including an overall reduction in the vasculature with fewer vessels and a lack of definitive capillaries (compare Fig. 7A, G) [44]. Loss of a single allele of *Smad4* in the *Vegfr2* null background (*Smad4*$^{f/+}$;*Vegfr2*$^{f/f}$-iECKO) resulted in similar phenotypes, suggesting that heterozygous loss of *Smad4* had little affect on the overall vascular phenotype (Fig. 7H). In addition, combinatorial deletion of *Smad4* and *Vegfr2* (*Smad4*$^{f/f}$;*Vegfr2*$^{f/f}$-iECKO) led to AVM formation, but these retinas exhibited very little vascular coverage (Fig. 7I). This suggests that there is a threshold for which loss of *Vegfr2* becomes dominant to *Smad4* deletion, as was previously reported in *Alk1* mutants [24]. In conclusion, our results indicate that reduction in VEGF signaling may contribute to heightened HHT phenotypes during developmental angiogenesis.

Discussion

Our studies are the first to report a *Smad4* animal model of HHT (*Smad4*-iECKO). We showed that endothelial loss of *Smad4* recapitulates vascular phenotypes seen in other HHT mouse models, particularly AVM formation. To better understand *Smad4*'s role in HHT pathogenesis, we performed a comprehensive characterization of *Smad4*-iECKO mice. Our results demonstrated that increased EC proliferation and size, alterations in mural cell coverage and disruption in AV gene expression are associated with *Smad4*-deficient blood vessels. We also provided evidence that loss of SMAD4 causes decreased VEGFR2 expression, and that loss of a single allele of *Vegfr2* in the *Smad4* null background leads to an increased severity of AVMs.

Considering *Smad4*'s centralized role in TGFβ signaling, we aimed to test the universality of our *Smad4*-iECKO model in relationship to HHT phenotypes. Consistent with previous reports, loss of TGFβ signaling through *Smad4* leads to vascular defects similar to those found in *Eng* and *Alk1* mouse retinal models (Fig. 1; summarized comparisons of HHT models in Table 1). For example, blood vessel enlargement in *Alk1* and *Eng* mutant mice has been linked to increases in EC proliferation [17, 20, 34, 45], which we also observed in our *Smad4* mutants (Fig. 2). Moreover, loss of *Smad4* led to an increase in EC cell size both in vivo and in vitro, which was unreported in *Alk1* and *Eng* models (Fig. 3). These findings are supported by a recent study showing that loss of *Smad4* caused an increase in the size and rates of proliferation of ECs in the coronary artery and under in vitro flow conditions [29]. Furthermore, work in zebrafish has shown that in response to increases in flow, *Eng*-deficient blood vessels enlarge [25]. Interestingly, our in vitro data suggest that, in *Smad4* mutants, cell size changes may also occur in the absence of flow. Taken together, it appears that blood vessel enlargement in HHT models is affected not only by increases in EC proliferation but also by an increase in EC size itself. How these alterations may lead to AVM formation is unclear, although it is notable that defects in the NOTCH pathway (both gain-of-function and loss-of-function) cause AVM formation [40, 41, 46, 47] via an initial increase in size of ECs [48]. Whether AVMs in HHT patients form in a similar manner remains an open question, as evidence in zebrafish suggests that HHT-associated AVMs are not directly caused by alterations in NOTCH signaling [49].

Nonetheless, our work demonstrated that expression of NOTCH signaling components, which are associated with arterial identity, as well as genes connected to venous and tip cell identity, are disrupted in the absence of *Smad4* (Fig. 4). We also revealed that these changes can occur in arteries, veins and/or capillaries; however, it is important to note that the AVMs themselves expressed all genes examined regardless of whether the marker was up- or downregulated in other vessel types. When comparing these results to those obtained in *Alk1* and *Eng* mouse models, we noted variations in AV gene expression between all three mutant backgrounds [17, 20, 24, 34, 38]. These differences could be due to tissue-specific effects related to the source tissues examined and/or the vascular expression patterns of *Alk1*, *Eng* and *Smad4*. For instance, some studies examined gene expression in isolated lung ECs [24], while others utilized brain and/or retinal ECs [20, 34]. Additionally, it is possible that expression levels in various vessel types play a role, as *Alk1* is highly expressed in arterial ECs [50], while *Eng* is only moderately expressed in arteries [51]. *Eng* also is expressed highly in capillaries and weakly in veins [52]. In comparison, *Smad4* is present in virtually all tissues [13, 14]. However, despite these differences, it is clear that overall disruptions in AV gene expression are consistent between all three mouse models of HHT. Further examination is

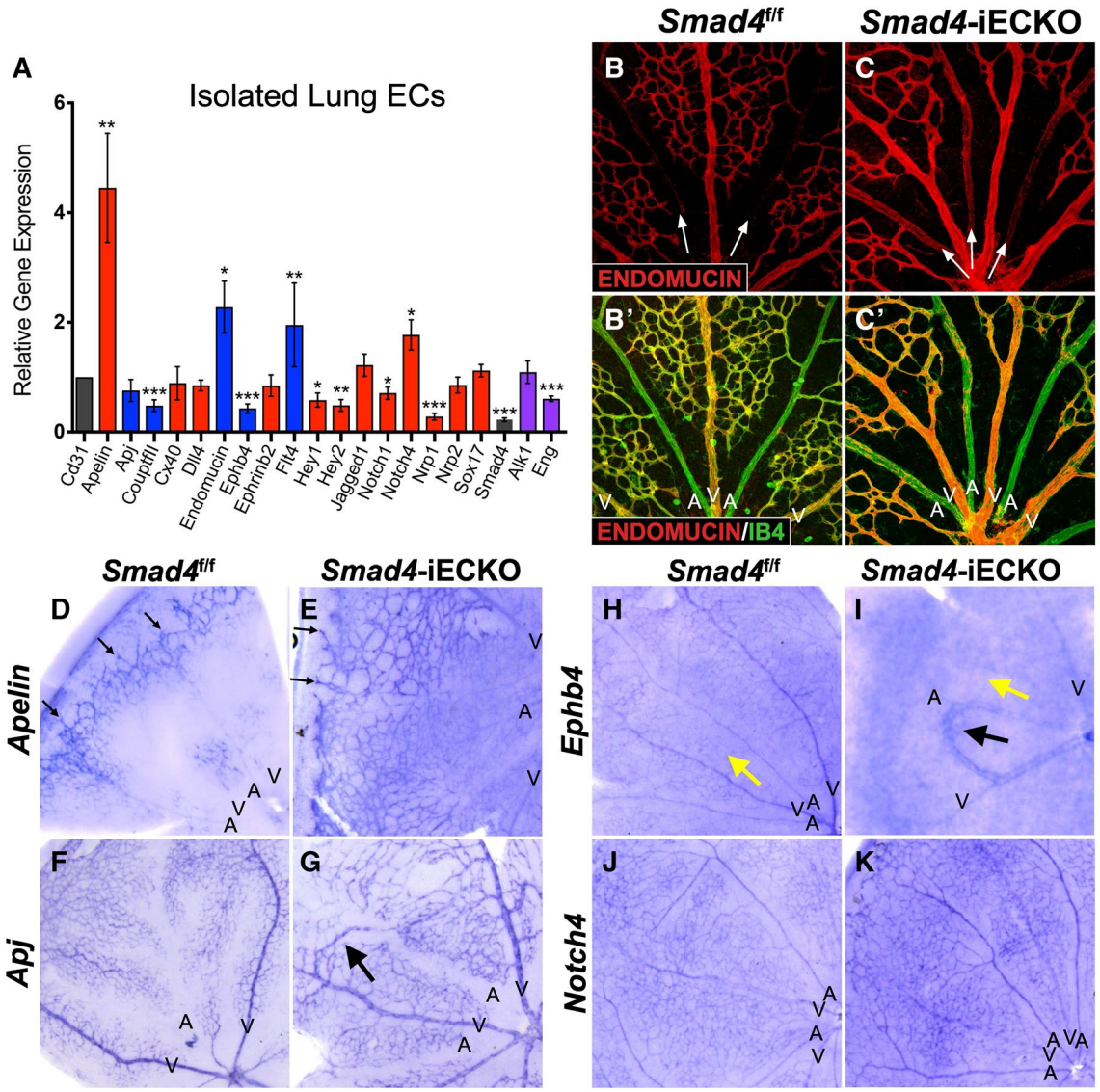

Fig. 5 *Smad4*-iECKO mice display alterations in artery and vein gene expression profiles. **A** qPCR analysis of 12 arterial (red), 5 venous (blue) and 2 HHT (purple)-associated genes on isolated, cultured lung ECs (iLECs) from P7 *Smad4*$^{f/f}$ ($n = 3$) and *Smad4*-iECKO ($n = 3$) mice revealed altered AV- and HHT-associated gene expression. All transcripts were normalized to *Cd31/Pecam* mRNA levels (*$p < 0.05$; **$p < 0.005$; ***$p \leq 0.0001$). **B**–**C**' Qualitative evaluation of *Smad4* control ($n = 6$) and mutant ($n = 6$) P7 retinas revealed increased levels of ENDOMUCIN protein (red) in arteries of *Smad4*-iECKO mice (white arrows; IB4, green). **D**–**K** In situ hybridization analysis of various artery–vein mRNAs substantiates qPCR results from iLECs. **D**, **E** *Apelin* mRNA is localized to the vascular tip cells (black arrows) and arteries of *Smad4*$^{f/f}$ mice ($n = 3$); however, in *Smad4*-iECKO mice *Apelin* is also robustly and ectopically expressed in the capillaries and veins ($n = 3$). **F**–**G** *Apj* expression remains unchanged in *Smad4*$^{f/f}$ ($n = 3$) and *Smad4*-iECKO ($n = 3$) littermate retinas. Arrow in **G** points to an AVM expressing *Apj*. **H**–**I** *Ephb4* mRNA is expressed strongly in the veins and moderately in the arteries and capillaries (yellow arrow) of *Smad4*$^{f/f}$ retinas ($n = 3$). In *Smad4*-iECKO retinas, *Ephb4* is largely absent in the capillary beds (yellow arrow) and in most arteries, excluding the artery connected to the AVM (black arrow) ($n = 3$). Note that *Ephb4* mRNA is expressed in the AVM. **J**–**K** *Notch4* mRNA expression patterns remain the same in *Smad4*$^{f/f}$ ($n = 3$) and *Smad4*-iECKO ($n = 3$) littermate retinas, but overall levels are increased in all vessel types of *Smad4* mutants. *a* arteries, *v* veins, *n* the number of independent biological samples

needed to address whether alterations in AV identity are a primary cause or secondary effect of AVM formation. To this point, our work does not address whether the observed phenotypes and molecular changes are a cause or an effect of AVM formation, as experiments were performed after AVMs developed. This cause/effect relationship has not been explored in *Alk1* and *Eng* models of HHT either. Therefore, future studies addressing this issue will be important for identifying the underlying molecular defects that drive AVM

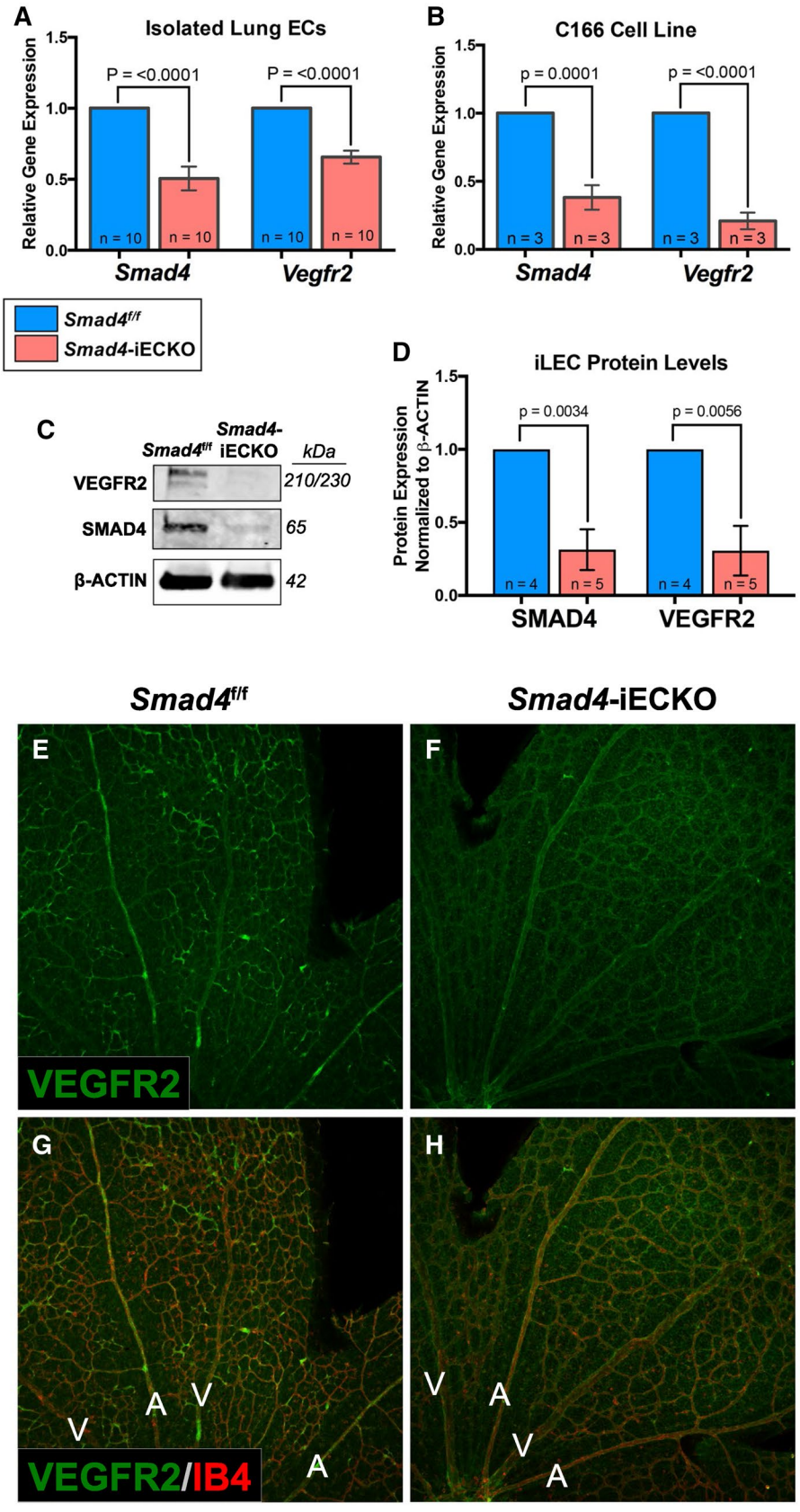

Fig. 6 Postnatal ablation of *Smad4* leads to reduced levels of *Vegfr2*. **A**, **B** qPCR analysis of *Smad4* and *Vegfr2* mRNA levels in isolated lung endothelial cells (**A**, normalized to *Cd31*) and C166 cells (**B**, normalized to *Odc*) reveals a significant reduction of *Vegfr2* transcripts when *Smad4* is knocked down. **C** Representative western blot shows reductions in SMAD4 and VEGFR2 proteins in *Smad4*-iECKO isolated lung ECs compared to $Smad4^{f/f}$ controls. **D** Western blot quantifications verify decreased VEGFR2 protein levels in *Smad4*-depleted iLECs. **E**–**F** Immunofluorescent staining of IB4 (red) and VEGFR2 (green) on P7 $Smad4^{f/f}$ ($n = 3$) and *Smad4*-iECKO ($n = 4$) retinas indicates reduced expression of VEGFR2 protein in *Smad4*-depleted blood vessels. Scale bar represents 200 µm. Sample size (n) represents the number of independent biological samples

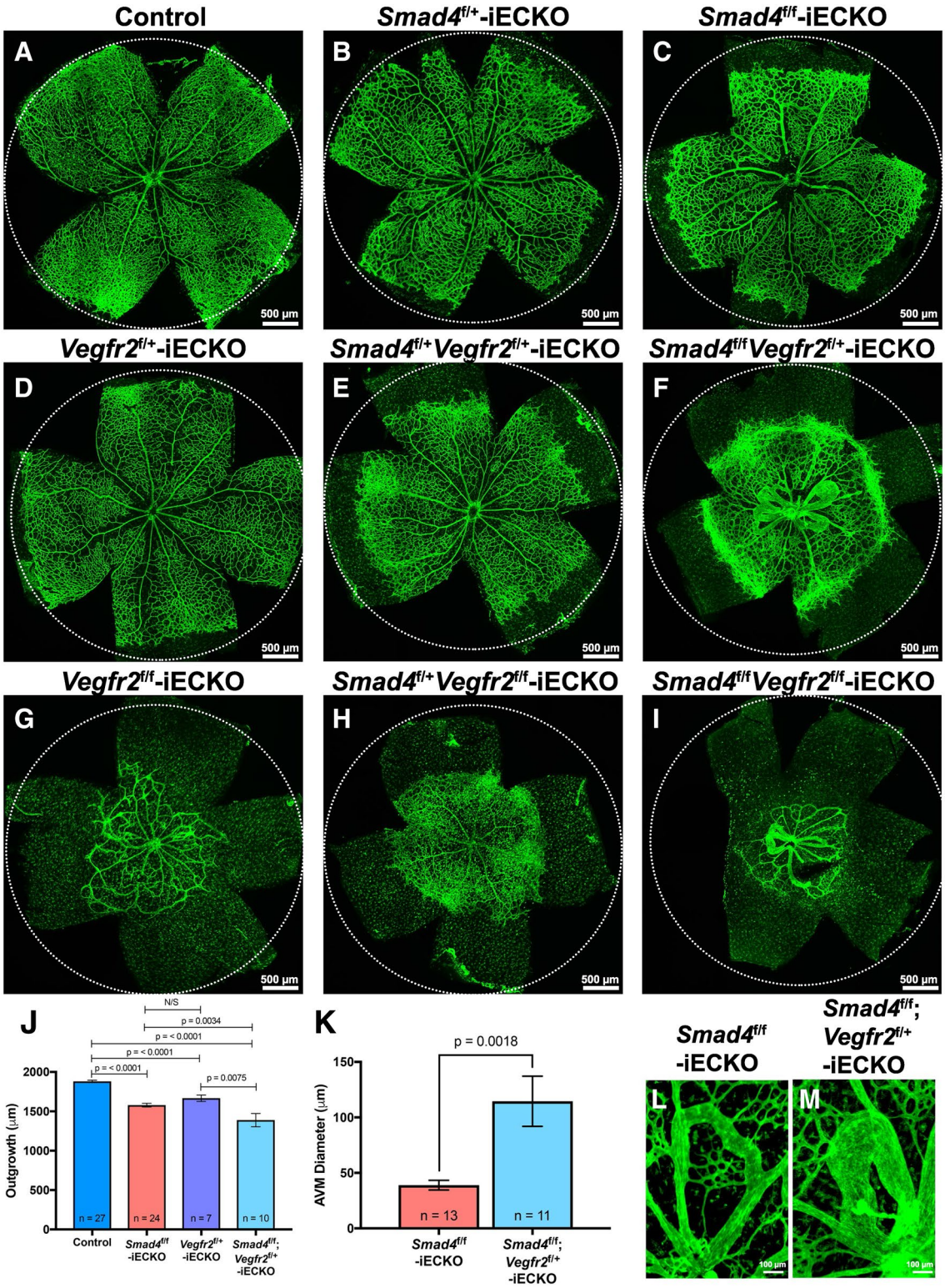

pathogenesis versus those that are secondary effects of AVM formation.

It is also important to note that tamoxifen-inducible murine models of HHT have several limitations. HHT phenotypes arise in patients due to mutations (most commonly missense mutations) that lead to haploinsufficiency [10]. In contrast, mouse models of HHT often utilize null genetic backgrounds because loss of one allele of *Alk1*, *Eng* or *Smad4* does not result in consistent presence of AVMs in predictable locations [21, 26, 53–55]. Furthermore, HHT

◂**Fig. 7** Postnatal ablation of *Smad4* and *Vegfr2* leads to enhanced AVM severity in the mouse retina. **A–I** Isolectin-IB4 staining (green) of P7 murine retinas from the following genotypes: **A** *Smad4*$^{f/f}$ control (n = 27), **B** *Smad4*$^{f/+}$-inducible endothelial cell knockout (iECKO) control (*Smad4*$^{f/+}$;*Cdh5*-Cre^{ERT2}) (n = 5), **C** *Smad4*$^{f/f}$-iECKO (n = 24), **D** *Vegfr2*$^{f/+}$-iECKO control (n = 7), **E** *Smad4*$^{f/+}$;*Vegfr2*$^{f/+}$-iECKO (n = 5), **F** *Smad4*$^{f/f}$;*Vegfr2*$^{f/+}$-iECKO (n = 14), **G** *Vegfr2*$^{f/f}$-iECKO (n = 3), **H** *Smad4*$^{f/+}$;*Vegfr2*$^{f/f}$-iECKO (n = 7) and **I** *Smad4*$^{f/f}$;*Vegfr2*$^{f/f}$-iECKO (n = 7). Dotted circles represent vascular outgrowth of the control retina in **A**. Scale bar represents 500 µm. **J** Quantification of vascular outgrowth in select genotypes revealed statistically significant decreases in *Smad4*$^{f/f}$;*Vegfr2*$^{f/+}$-iECKO retinas. **K** *Smad4*$^{f/f}$;*Vegfr2*$^{f/+}$-iECKO mice exhibit an increased AVM severity as measured by AVM diameter. **L, M** Close-up views comparing AVMs in *Smad4*-iECKO and *Smad4*$^{f/f}$;*Vegfr2*$^{f/+}$-iECKO retinas

patients harbor germline mutations, which manifest from gestation and remain throughout adulthood. However, in mice, complete loss of *Alk1*, *Eng* or *Smad4* during gestation results in embryonic lethality making it impossible to study their postnatal impact on HHT [16, 27, 33, 56, 57]. For this reason, the mouse retina has become an effective model to study AVM formation; the retinal vasculature forms directly after birth allowing researchers to assess developmental angiogenesis, similar to vessel growth that would be seen in a developing human. Although these models do not perfectly mimic the genetic background of HHT patients, retinal AVMs form at consistent rates and locations providing a reliable model to investigate the mechanisms of AVM formation.

In our *Smad4*-iECKO retinas we noted delayed angiogenic outgrowth similar to *Eng* mutants [17, 34], while *Alk1* mutant retinas did not exhibit reduction in vascular outgrowth [20]. Interestingly, our *Smad4*-iECKO mice exhibit a significant reduction in *Eng* transcript levels but show no changes in *Alk1* mRNA levels (Fig. 5A). This could account for the observed similarities in reduced vascular outgrowth between *Smad4* and *Eng*, but not *Alk1* mice. However, this result also illustrates the complex association

Table 1 Comparison of HHT mouse models

Mutation	*Alkl*	*Eng*	*Smad4*
Associated with	HHT2	HHT1	HHT/JP
Percentage of mutants with AVMs	60% [20]	70% [17]	82%
Angiogenic delay	No reduction [20]	Reduced [1, 34]	Reduced
Vessel size			
Artery size		Enlarged [34]	Enlarged
Vein size	Enlarged [20]	Enlarged [17]	Enlarged
Proliferation in			
Artery		Increased [17, 34]	Increased
Vein	Increased [20]	Increased [17], not changed [34]	Increased
Capillary		Increased [17], not changed [34]	Increased
Cell size			Increased [29][a]
Smooth muscle coverage	Increased [20]	Increased [17]	Increased
Pericytes	Decreased (only in capillaries) [20]		Decreased
Artery identity			
Dll4		No change [34]; not expressed in AVM	No change
Ephrinb2	Downregulated[??]	No change [17], downregulated [34]	No change
Hey1		Downregulated [34]	Downregulated
Jagged1	Downregulated [20, 24]	No change [17]; increased [34]	No change
Notch1	Downregulated [20, 24]		Downregulated
Venous identity			
Apj	No change [17]; upregulated [24]	No change (Expressed in AVM) [34]	No change; expressed in AVM
Ephb4		No change (Expressed in AVM) [34]	Reduced expressed in AVM
VEGFR2 levels	No change [24]	Altered VEGFA-induced kinetics [34]	Downregulated
Respiratory distress	24–48 h post-Tx Inj [20]		168–192 h post-Tx Inj

This table combines data from references using the inducible, endothelial-specific Cre-driver line Cdh5-Cre^{ERT2}: Mahmoud et al. [17], Tual-Chalot et al. [20], Ola et al. [24], Jin et al. [34] and Poduri et al. [29]

[a]Note that Poduri et al. [29] used a ubiquitous *Rosa*-Cre^{ER} driver line. No in vitro data were included in this table

between the TGFβ pathway and HHT, as *Eng* expression levels are reduced in the *Alk1* mouse models of HHT [20, 24], yet show no changes in outgrowth. To our knowledge, it is unknown what happens to levels of *Alk1* expression in the *Eng* HHT model, or whether *Smad4* levels are affected in either *Alk1* or *Eng* mouse models. Moving forward, it will be important to understand the association between *Alk1*, *Eng* and *Smad4* in HHT because even though it is expected that all three cooperate in a linear manner in the TGFβ pathway, differences in phenotypes (Table 1) suggest this might not be the case.

The overall objective of our work was to develop a *Smad4* model of HHT that could be used to identify the TGFβ targets that drive AVM formation, as almost nothing is known about these downstream effectors. To this end, we explored a possible link with the vascular endothelial growth factor (VEGF) signaling pathway that has been previously suggested in other HHT models [21, 24, 26, 34, 42, 53]. For instance, homozygous-induced deletion of *Alk1* or *Eng* in adult mice requires the presence of exogenous VEGF before AVMs will form in the brain, suggesting that activation of the VEGF pathway is needed for AVM formation [21, 26]. To this end, VEGF neutralizing antibodies have been shown to prevent wound-induced skin AVMs from developing in *Alk1*-deficient mice [53]. Furthermore, in the absence of *Alk1* and *Eng*, several studies have reported increased *Vegfr2* expression and altered VEGFR2 kinetics in vitro [24, 34, 42]. In contrast, our data showed that loss of *Smad4* led to a reliable and significant decrease in *Vegfr2* expression both in vitro and in vivo (Fig. 6). This is consistent with a previous study on human patients with cerebral brain AVMs where there was a marked decrease in *Vegfr2* expression [58]. Contrary to other HHT studies, the reduction of *Vegfr2* in *Smad4*-iECKO mice could potentially be attributed to the downregulation in *Nrp1*, a VEGFR2 co-receptor. Studies have shown that decreased *Nrp1* levels correlate with reduced *Vegfr2* expression [59, 60]. Although other HHT studies did not find reduced *Vegfr2* levels, homozygous deletion of both *Smad4* and *Vegfr2* produced similar results to those obtained in double *Alk1*- and *Vegfr2*-deficient retinas [24]. In each study, deletion of both alleles of *Vegfr2* in the *Alk1* or *Smad4* null backgrounds resulted in inhibition of retinal vascular development, suggesting that appreciable loss of *Vegfr2* in the absence of either *Alk1* or *Smad4* overrides HHT-like phenotypes because the vasculature is severely underdeveloped (Fig. 7). We did note that AVMs still formed in both experiments at fewer and similar rates in *Alk1* and *Smad4* mutants, respectively. However, in further studies we demonstrated that loss of a single *Vegfr2* allele in the *Smad4* mutant background led to an enhancement of vascular phenotypes associated with *Smad4*-iECKO retinas; the vascular front exhibited a consistent increase in density and AVMs showed a substantial enlargement. Alternatively, increased AVM size could be attributed to altered blood flow rates, hemodynamics forces and/or rates of oxygen diffusion caused by the overall stunted growth of the mutant blood vessels, rather than due to the loss of VEGFR2 directly. Future studies will be needed to understand how these processes are altered in TGFβ mutant backgrounds and how those contributions may affect severity of AVMs.

This SMAD4-VEGFR2 association is somewhat contrary to the clinical use of bevacizumab (also known as Avastin), which is a humanized anti-VEGF monoclonal antibody that sequesters VEGF to prevent it from binding both VEGFR1 and VEGFR2 subsequently hindering angiogenesis [61, 62]. Bevacizumab is currently used as a palliative therapy for HHT where it alleviates symptoms such as chronic nosebleeds but is not considered a long-term therapy [63]. Studies on the use of bevacizumab have been performed in mature vascular networks, namely that of adult humans and mice [64, 65]. Little information is known about the effects of bevacizumab in children or developing/remodeling vascular networks. Our work suggests that the connection between SMAD4 and VEGFR2 is different during developmental angiogenesis, when AVMs are thought to form, as compared to mature, established vascular networks. Therefore, further research on the effects of bevacizumab in developing vascular networks is needed, as our results indicate that bevacizumab may enhance developmental HHT phenotypes.

Materials and methods

Mice

All animal experiments were performed in accordance with Tulane University's Institutional Animal Care and Use Committee policy. To create our *Smad4*-iECKO mouse model, we crossed an endothelial-specific, tamoxifen-inducible Cre-driver line (Tg(Cdh5-Cre^{ERT2})^{1Rha}, further referred to as *Cdh5*-Cre^{ERT2}) [30] with a conditional Smad4 mouse (Smad4$^{f/f}$) [31]. To confirm that *Smad4* was being knocked out only in ECs, we mated *Smad4*-iECKO mice with a *Rosa26*-EYFP reporter mouse (Gt(ROSA)26Sor$^{tm1(EYFP)Cos}$) [32]. Induction of tamoxifen was done using 0.075 mg tamoxifen (Sigma T5648) per gram of body weight on postnatal days 1 and 4. Note: For *Vegfr2*-iECKO mice only one injection of Tx was given on P1. For experiments, *Smad4*$^{f/f}$;*Cdh5*-Cre^{ERT2} (otherwise referred to as *Smad4*-iECKO) mice were the experimental group, while *Smad4*$^{f/f}$ littermates were used as controls. Genotyping primers and conditions can be found in supplemental methods.

Hematoxylin and eosin staining of murine lungs

Neonatal lungs were dissected from postnatal day 8 pups and fixed for 4 h in 4% PFA at 4 °C. The lungs were then embedded in paraffin and sectioned at 10 µm. Sections were washed in xylenes twice then put through a rehydration series. Slides were placed into hematoxylin solution for ~ 1 min and then rinsed with water for several minutes. This process was repeated for eosin staining. Slides were then mounted with Permount (Thermo).

Retinal whole mount stains

Retinas were dissected and stained as previously described [66]. The following antibodies were used at a 1:100 concentration: αSMA (Sigma C6198), cleaved CASPASE-3 (Cell signaling 9661), COLLAGEN IV (Millipore AB756P), ENDOMUCIN (Santa Cruz 6415), ERG (Abcam 92513), GFP (Aves GFP-1020), KI67 (Cell Signaling 9449), NG2 (Millipore 5320), PECAM/CD31 (BD 553370), VEGFR2 (BD 555307). Additionally, the following immunofluorescent stains were performed according to the manufacturer's instructions: Dapi (Life Technologies R37606), Isolectin-488 (Invitrogen 21411), Isolectin-594 (Invitrogen 21413), Isolectin-647 (Invitrogen 32450). Confocal images were taken at the same exposure settings for both mutant and control retinas, so fluorescent intensity could be compared.

In situ hybridizations

In situ hybridizations were performed as previously described [66]. In situ hybridizations were performed in batches where mutants and controls were subjected to the colorimetric reaction for the same period of time so that results could be compared. The following probes were synthesized from plasmids containing: *Apelin* (Dharmacon), *Apj* (Dharmacon), *Ephb4*, *Notch4*. Images were taken using a Leica M205 FA stereomicroscope.

Isolation of endothelial cells

Retinal and lung endothelial cell isolation were performed as previously described [67]. Briefly, tissue (either lung or retina) was digested in a collagenase/dispase solution and minced into fine pieces. After obtaining a single cell suspension, sheep anti-rat IgG dynabeads (Invitrogen 11035) coated with PECAM/CD31 antibody (BD 553370) were used to isolate endothelial cells. Cells were either used for RNA collection immediately or allowed to grow in EGM-2 medium for one week before being used for protein or RNA collection.

qPCR and analysis

All quantitative real-time PCR (qPCR) experiments were performed using RNA isolated with a GeneJET RNA Purification Kit (Thermo K0732) and quantified using a Nanodrop (Thermo). For each sample, 500–1000 ng of RNA was used for cDNA synthesis using a iScript cDNA Synthesis Kit (Bio-Rad). qPCRs were run using SYBR green mastermix (Thermo K0221) on a Bio-Rad CFX96 Touch Real-Time PCR Detection machine. Analysis was performed using the double delta Ct method, and statistics were generated using GraphPad Prism. For all qPCR experiments, three independent biological replicates were used and three technical replicates were performed per sample. Primers were verified for specificity and efficiency and can be found in supplemental materials.

Quantification of retinal images

All retina images were analyzed using Nikon NIS-Elements AR Analysis 64-bit software, and ImageJ software was used to measure vascular outgrowth, cell area and cell density.

Statistical analysis

GraphPad Prism software was used for all statistical analysis. For all statistics, sample size (n) indicates the number of independent biological samples. A minimum of three technical replicates was included per sample. For statistical analysis, we ran unpaired two-tailed Student's t test where a p value of < 0.05 was considered significant.

Acknowledgements We would like to thank Masanori Hirashima and Ralf Adams for the use of the Vegfr2-floxed and Cdh5-Cre^{ERT2} mice, respectively. The Notch4 and EphB4 in situ plasmids were supplied from Ondine Cleaver. This work was supported by start-up funds from Tulane University, funds from the Tulane Committee of Research, and the Department of Defense Investigator-Initiated Research Award (PRMRP160198) [S.M.M.]. This work was supported by funds from the Louisiana Board of Reagents [A.M.C.]. We would also like to acknowledge Harvard Primer Bank and NCBI Primer-Blast for primers used in qPCRs.

Compliance with ethical standards

Conflict of interest We have no competing financial interests.

References

1. Kjeldsen AD, Vase P, Green A (1999) Hereditary haemorrhagic telangiectasia: a population-based study of prevalence and mortality in Danish patients. J Intern Med 245(1):31–39
2. Dakeishi M, Shioya T, Wada Y, Shindo T, Otaka K, Manabe M, Nozaki J, Inoue S, Koizumi A (2002) Genetic epidemiology of hereditary hemorrhagic telangiectasia in a local community in the northern part of Japan. Hum Mutat 19(2):140–148. https://doi.org/10.1002/humu.10026
3. Shovlin CL (2010) Hereditary haemorrhagic telangiectasia: pathophysiology, diagnosis and treatment. Blood Rev 24(6):203–219. https://doi.org/10.1016/j.blre.2010.07.001
4. Botella LM, Albinana V, Ojeda-Fernandez L, Recio-Poveda L, Bernabeu C (2015) Research on potential biomarkers in hereditary hemorrhagic telangiectasia. Front Genet 6:115. https://doi.org/10.3389/fgene.2015.00115
5. Sabba C, Pasculli G, Suppressa P, D'Ovidio F, Lenato GM, Resta F, Assennato G, Guanti G (2006) Life expectancy in patients with hereditary haemorrhagic telangiectasia. QJM Mon J Assoc Phys 99(5):327–334. https://doi.org/10.1093/qjmed/hcl037
6. Alberici P, Gaspar C, Franken P, Gorski MM, de Vries I, Scott RJ, Ristimaki A, Aaltonen LA, Fodde R (2008) Smad4 haploinsufficiency: a matter of dosage. PathoGenetics 1(1):2. https://doi.org/10.1186/1755-8417-1-2
7. Govani FS, Shovlin CL (2009) Hereditary haemorrhagic telangiectasia: a clinical and scientific review. Eur J Hum Genet EJHG 17(7):860–871. https://doi.org/10.1038/ejhg.2009.35
8. Grosse SD, Boulet SL, Grant AM, Hulihan MM, Faughnan ME (2014) The use of US health insurance data for surveillance of rare disorders: hereditary hemorrhagic telangiectasia. Genet ed 16(1):33–39. https://doi.org/10.1038/gim.2013.66
9. Bayrak-Toydemir P, McDonald J, Markewitz B, Lewin S, Miller F, Chou LS, Gedge F, Tang W, Coon H, Mao R (2006) Genotype-phenotype correlation in hereditary hemorrhagic telangiectasia: mutations and manifestations. Am J Med Genet Part A 140(5):463–470. https://doi.org/10.1002/ajmg.a.31101
10. McDonald J, Wooderchak-Donahue W, VanSant Webb C, Whitehead K, Stevenson DA, Bayrak-Toydemir P (2015) Hereditary hemorrhagic telangiectasia: genetics and molecular diagnostics in a new era. Front Genet 6:1. https://doi.org/10.3389/fgene.2015.00001
11. Gallione CJ, Richards JA, Letteboer TG, Rushlow D, Prigoda NL, Leedom TP, Ganguly A, Castells A, Ploos van Amstel JK, Westermann CJ, Pyeritz RE, Marchuk DA (2006) SMAD4 mutations found in unselected HHT patients. J Med Genet 43(10):793–797. https://doi.org/10.1136/jmg.2006.041517
12. Gallione C, Aylsworth AS, Beis J, Berk T, Bernhardt B, Clark RD, Clericuzio C, Danesino C, Drautz J, Fahl J, Fan Z, Faughnan ME, Ganguly A, Garvie J, Henderson K, Kini U, Leedom T, Ludman M, Lux A, Maisenbacher M, Mazzucco S, Olivieri C, Ploos van Amstel JK, Prigoda-Lee N, Pyeritz RE, Reardon W, Vandezande K, Waldman JD, White RI Jr, Williams CA, Marchuk DA (2010) Overlapping spectra of SMAD4 mutations in juvenile polyposis (JP) and JP-HHT syndrome. Am J Med GenetPart A 152a(2):333–339. https://doi.org/10.1002/ajmg.a.33206
13. Luukko K, Ylikorkala A, Makela TP (2001) Developmentally regulated expression of Smad3, Smad4, Smad6, and Smad7 involved in TGF-beta signaling. Mech Dev 101(1–2):209–212
14. Yue F, Cheng Y, Breschi A, Vierstra J, Wu W, Ryba T, Sandstrom R, Ma Z, Davis C, Pope BD, Shen Y, Pervouchine DD, Djebali S, Thurman RE, Kaul R, Rynes E, Kirilusha A, Marinov GK, Williams BA, Trout D, Amrhein H, Fisher-Aylor K, Antoshechkin I, DeSalvo G, See LH, Fastuca M, Drenkow J, Zaleski C, Dobin A, Prieto P, Lagarde J, Bussotti G, Tanzer A, Denas O, Li K, Bender MA, Zhang M, Byron R, Groudine MT, McCleary D, Pham L, Ye Z, Kuan S, Edsall L, Wu YC, Rasmussen MD, Bansal MS, Kellis M, Keller CA, Morrissey CS, Mishra T, Jain D, Dogan N, Harris RS, Cayting P, Kawli T, Boyle AP, Euskirchen G, Kundaje A, Lin S, Lin Y, Jansen C, Malladi VS, Cline MS, Erickson DT, Kirkup VM, Learned K, Sloan CA, Rosenbloom KR, Lacerda de Sousa B, Beal K, Pignatelli M, Flicek P, Lian J, Kahveci T, Lee D, Kent WJ, Ramalho Santos M, Herrero J, Notredame C, Johnson A, Vong S, Lee K, Bates D, Neri F, Diegel M, Canfield T, Sabo PJ, Wilken MS, Reh TA, Giste E, Shafer A, Kutyavin T, Haugen E, Dunn D, Reynolds AP, Neph S, Humbert R, Hansen RS, De Bruijn M, Selleri L, Rudensky A, Josefowicz S, Samstein R, Eichler EE, Orkin SH, Levasseur D, Papayannopoulou T, Chang KH, Skoultchi A, Gosh S, Disteche C, Treuting P, Wang Y, Weiss MJ, Blobel GA, Cao X, Zhong S, Wang T, Good PJ, Lowdon RF, Adams LB, Zhou XQ, Pazin MJ, Feingold EA, Wold B, Taylor J, Mortazavi A, Weissman SM, Stamatoyannopoulos JA, Snyder MP, Guigo R, Gingeras TR, Gilbert DM, Hardison RC, Beer MA, Ren B, Mouse EC (2014) A comparative encyclopedia of DNA elements in the mouse genome. Nature 515(7527):355–364. https://doi.org/10.1038/nature13992
15. Massague J (2012) TGF-beta signaling in development and disease. FEBS Lett 586(14):1833. https://doi.org/10.1016/j.febslet.2012.05.030
16. Urness LD, Sorensen LK, Li DY (2000) Arteriovenous malformations in mice lacking activin receptor-like kinase-1. Nat Genet 26(3):328–331. https://doi.org/10.1038/81634
17. Mahmoud M, Allinson KR, Zhai Z, Oakenfull R, Ghandi P, Adams RH, Fruttiger M, Arthur HM (2010) Pathogenesis of arteriovenous malformations in the absence of endoglin. Circ Res 106(8):1425–1433. https://doi.org/10.1161/CIRCRESAHA.109.211037
18. Park SO, Wankhede M, Lee YJ, Choi EJ, Fliess N, Choe SW, Oh SH, Walter G, Raizada MK, Sorg BS, Oh SP (2009) Real-time imaging of de novo arteriovenous malformation in a mouse model of hereditary hemorrhagic telangiectasia. J Clin Investig 119(11):3487–3496. https://doi.org/10.1172/jci39482
19. Corti P, Young S, Chen CY, Patrick MJ, Rochon ER, Pekkan K, Roman BL (2011) Interaction between alk1 and blood flow in the development of arteriovenous malformations. Development 138(8):1573–1582. https://doi.org/10.1242/dev.060467
20. Tual-Chalot S, Mahmoud M, Allinson KR, Redgrave RE, Zhai Z, Oh SP, Fruttiger M, Arthur HM (2014) Endothelial depletion of Acvrl1 in mice leads to arteriovenous malformations associated with reduced endoglin expression. PLoS ONE 9(6):e98646. https://doi.org/10.1371/journal.pone.0098646
21. Choi EJ, Chen W, Jun K, Arthur HM, Young WL, Su H (2014) Novel brain arteriovenous malformation mouse models for type 1 hereditary hemorrhagic telangiectasia. PLoS ONE 9(2):e88511. https://doi.org/10.1371/journal.pone.0088511
22. Arthur H, Geisthoff U, Gossage JR, Hughes CC, Lacombe P, Meek ME, Oh P, Roman BL, Trerotola SO, Velthuis S, Wooderchak-Donahue W (2015) Executive summary of the 11th HHT international scientific conference. Angiogenesis 18(4):511–524. https://doi.org/10.1007/s10456-015-9482-5
23. Ruiz S, Zhao H, Chandakkar P, Chatterjee PK, Papoin J, Blanc L, Metz CN, Campagne F, Marambaud P (2016) A mouse model of hereditary hemorrhagic telangiectasia generated by transmammary-delivered immunoblocking of BMP9 and BMP10. Sci Rep 5:37366. https://doi.org/10.1038/srep37366
24. Ola R, Dubrac A, Han J, Zhang F, Fang JS, Larrivee B, Lee M, Urarte AA, Kraehling JR, Genet G, Hirschi KK, Sessa WC, Canals FV, Graupera M, Yan M, Young LH, Oh PS, Eichmann A (2016) PI3 kinase inhibition improves vascular malformations

in mouse models of hereditary haemorrhagic telangiectasia. Nat Commun 7:13650. https://doi.org/10.1038/ncomms13650
25. Sugden WW, Meissner R, Aegerter-Wilmsen T, Tsaryk R, Leonard EV, Bussmann J, Hamm MJ, Herzog W, Jin Y, Jakobsson L, Denz C, Siekmann AF (2017) Endoglin controls blood vessel diameter through endothelial cell shape changes in response to haemodynamic cues. Nat Cell Biol 19(6):653–665. https://doi.org/10.1038/ncb3528
26. Chen W, Young W, Su H (2014) Induction of brain arteriovenous malformation in the adult mouse. Methods Mol Biol 1135:309–316
27. Lan Y, Liu B, Yao H, Li F, Weng T, Yang G, Li W, Cheng X, Mao N, Yang X (2007) Essential role of endothelial Smad4 in vascular remodeling and integrity. Mol Cell Biol 27(21):7683–7692. https://doi.org/10.1128/MCB.00577-07
28. Li F, Lan Y, Wang Y, Wang J, Yang G, Meng F, Han H, Meng A, Wang Y, Yang X (2011) Endothelial Smad4 maintains cerebrovascular integrity by activating N-cadherin through cooperation with Notch. Dev Cell 20(3):291–302. https://doi.org/10.1016/j.devcel.2011.01.011
29. Poduri A, Chang AH, Raftrey B, Rhee S, Van M, Red-Horse K (2017) Endothelial cells respond to the direction of mechanical stimuli through SMAD signaling to regulate coronary artery size. Development (Camb, Engl) 144(18):3241–3252. https://doi.org/10.1242/dev.150904
30. Wang Y, Nakayama M, Pitulescu ME, Schmidt TS, Bochenek ML, Sakakibara A, Adams S, Davy A, Deutsch U, Luthi U, Barberis A, Benjamin LE, Makinen T, Nobes CD, Adams RH (2010) Ephrin-B2 controls VEGF-induced angiogenesis and lymphangiogenesis. Nature 465(7297):483–486. https://doi.org/10.1038/nature09002
31. Yang X, Li C, Herrera PL, Deng CX (2002) Generation of Smad4/Dpc4 conditional knockout mice. Genesis 32(2):80–81
32. Srinivas SWT, Lin C, William C, Tanabe Y, Jessell TM, Costantini F (2004) Cre reporter strains produced by targeted insertion of EYFP and ECFP into the ROSA26 locus. BMC Dev Biol 1:4
33. Oh PSP, Goss KA, Imamura T, Yi Y, Donahoe PK, Li L, Miyazono K, Dijke P, Kim S, Li E (2000) Activin receptor-like kinase 1 modulates transforming growth factor- 1 signaling in the regulation of angiogenesis. PNAS 97(6):2626–2631
34. Jin Y, Muhl L, Burmakin M, Wang Y, Duchez AC, Betsholtz C, Arthur HM, Jakobsson L (2017) Endoglin prevents vascular malformation by regulating flow-induced cell migration and specification through VEGFR2 signalling. Nat Cell Biol 19(6):639–652. https://doi.org/10.1038/ncb3534
35. Baeyens N, Larrivee B, Ola R, Hayward-Piatkowskyi B, Dubrac A, Huang B, Ross TD, Coon BG, Min E, Tsarfati M, Tong H, Eichmann A, Schwartz MA (2016) Defective fluid shear stress mechanotransduction mediates hereditary hemorrhagic telangiectasia. J Cell Biol 214(7):807–816. https://doi.org/10.1083/jcb.201603106
36. Rochon ER, Menon PG, Roman BL (2016) Alk1 controls arterial endothelial cell migration in lumenized vessels. Development 143(14):2593–2602. https://doi.org/10.1242/dev.135392
37. Armulik A, Genove G, Betsholtz C (2011) Pericytes: developmental, physiological, and pathological perspectives, problems, and promises. Dev Cell 21(2):193–215. https://doi.org/10.1016/j.devcel.2011.07.001
38. Larrivee B, Prahst C, Gordon E, del Toro R, Mathivet T, Duarte A, Simons M, Eichmann A (2012) ALK1 signaling inhibits angiogenesis by cooperating with the Notch pathway. Dev Cell 22(3):489–500. https://doi.org/10.1016/j.devcel.2012.02.005
39. Atri D, Larrivee B, Eichmann A, Simons M (2013) Endothelial signaling and the molecular basis of arteriovenous malformation. Cell Mol Life Sci. https://doi.org/10.1007/s00018-013-1475-1
40. Krebs LT, Shutter JR, Tanigaki K, Honjo T, Stark KL, Gridley T (2004) Haploinsufficient lethality and formation of arteriovenous malformations in Notch pathway mutants. Genes Dev 18(20):2469–2473. https://doi.org/10.1101/gad.1239204
41. Nielsen CM, Cuervo H, Ding VW, Kong Y, Huang EJ, Wang RA (2014) Deletion of Rbpj from postnatal endothelium leads to abnormal arteriovenous shunting in mice. Development 141(19):3782–3792. https://doi.org/10.1242/dev.108951
42. Ruiz S, Chandakkar P, Zhao H, Papoin J, Chatterjee PK, Christen E, Metz CN, Blanc L, Campagne F, Marambaud P (2017) Tacrolimus rescues endothelial ALK1 loss-of-function signaling and improves HHT vascular pathology. https://doi.org/10.1101/137737
43. Albuquerque RJ, Hayashi T, Cho WG, Kleinman ME, Dridi S, Takeda A, Baffi JZ, Yamada K, Kaneko H, Green MG, Chappell J, Wilting J, Weich HA, Yamagami S, Amano S, Mizuki N, Alexander JS, Peterson ML, Brekken RA, Hirashima M, Capoor S, Usui T, Ambati BK, Ambati J (2009) Alternatively spliced vascular endothelial growth factor receptor-2 is an essential endogenous inhibitor of lymphatic vessel growth. Nat Med 15(9):1023–1030. https://doi.org/10.1038/nm.2018
44. Zarkada G, Heinolainen K, Makinen T, Kubota Y, Alitalo K (2015) VEGFR3 does not sustain retinal angiogenesis without VEGFR2. Proc Natl Acad Sci USA 112(3):761–766. https://doi.org/10.1073/pnas.1423278112
45. Lebrin F, Goumans MJ, Jonker L, Carvalho RL, Valdimarsdottir G, Thorikay M, Mummery C, Arthur HM, ten Dijke P (2004) Endoglin promotes endothelial cell proliferation and TGF-beta/ALK1 signal transduction. EMBO J 23(20):4018–4028. https://doi.org/10.1038/sj.emboj.7600386
46. Carlson TR, Yan Y, Wu X, Lam MT, Tang GL, Beverly LJ, Messina LM, Capobianco AJ, Werb Z, Wang R (2005) Endothelial expression of constitutively active Notch4 elicits reversible arteriovenous malformations in adult mice. Proc Natl Acad Sci USA 102(28):9884–9889. https://doi.org/10.1073/pnas.0504391102
47. Krebs LT, Starling C, Chervonsky AV, Gridley T (2010) Notch1 activation in mice causes arteriovenous malformations phenocopied by ephrinB2 and EphB4 mutants. Genesis (NY) 48(3):146–150. https://doi.org/10.1002/dvg.20599
48. Murphy PA, Kim TN, Huang L, Nielsen CM, Lawton MT, Adams RH, Schaffer CB, Wang RA (2014) Constitutively active Notch4 receptor elicits brain arteriovenous malformations through enlargement of capillary-like vessels. Proc Natl Acad Sci USA 111(50):18007–18012. https://doi.org/10.1073/pnas.1415316111
49. Rochon ER, Wright DS, Schubert MM, Roman BL (2015) Context-specific interactions between Notch and ALK1 cannot explain ALK1-associated arteriovenous malformations. Cardiovasc Res 107(1):143–152. https://doi.org/10.1093/cvr/cvv148
50. Seki T, Yun J, Oh SP (2003) Arterial endothelium-specific activin receptor-like kinase 1 expression suggests its role in arterialization and vascular remodeling. Circ Res 93(7):682–689. https://doi.org/10.1161/01.RES.0000095246.40391.3B
51. Jonker L, Arthur HM (2002) Endoglin expression in early development is associated with vasculogenesis and angiogenesis. Mech Dev 110(1–2):193–196
52. LaAH Jonker (2002) Endoglin expression in early development is associated with vasculogenesis and angiogenesis. Mech Dev 110:193–196
53. Han C, Choe SW, Kim YH, Acharya AP, Keselowsky BG, Sorg BS, Lee YJ, Oh SP (2014) VEGF neutralization can prevent and normalize arteriovenous malformations in an animal model for hereditary hemorrhagic telangiectasia 2. Angiogenesis 17(4):823–830. https://doi.org/10.1007/s10456-014-9436-3
54. Gkatzis K, Thalgott J, Dos-Santos-Luis D, Martin S, Lamande N, Carette MF, Disch F, Snijder RJ, Westermann CJ, Mager JJ, Oh SP, Miquerol L, Arthur HM, Mummery CL, Lebrin F (2016)

Interaction between ALK1 signaling and Connexin40 in the development of arteriovenous malformations. Arterioscler Thromb Vasc Biol 36(4):707–717. https://doi.org/10.1161/ATVBAHA.115.306719
55. Satomi J, Mount RJ, Toporsian M, Paterson AD, Wallace MC, Harrison RV, Letarte M (2003) Cerebral vascular abnormalities in a murine model of hereditary hemorrhagic telangiectasia. Stroke 34(3):783–789. https://doi.org/10.1161/01.STR.0000056170.47815.37
56. Bourdeau A, Dumont DJ, Letarte M (1999) A murine model of hereditary hemorrhagic telangiectasia. J Clin Invest 104(10):1343–1351. https://doi.org/10.1172/JCI8088
57. Li DY, Sorensen LK, Brooke BS, Urness LD, Davis EC, Taylor DG, Boak BB, Wendel DP (1999) Defective angiogenesis in micelacking endoglin. Science 284(55419):1534–1537
58. Hashimoto T, Emala CW, Joshi S, Mesa-Tejada R, Quick CM, Feng L, Libow A, Marchuk DA, Young WL (2000) Abnormal pattern of Tie-2 and vascular endothelial growth factor receptor expression in human cerebral arteriovenous malformations. Neurosurgery 47(4):910–918
59. Gelfand MV, Hagan N, Tata A, Oh WJ, Lacoste B, Kang KT, Kopycinska J, Bischoff J, Wang JH, Gu C (2014) Neuropilin-1 functions as a VEGFR2 co-receptor to guide developmental angiogenesis independent of ligand binding. eLife 3:e03720. https://doi.org/10.7554/elife.03720
60. Raimondi C, Fantin A, Lampropoulou A, Denti L, Chikh A, Ruhrberg C (2014) Imatinib inhibits VEGF-independent angiogenesis by targeting neuropilin 1-dependent ABL1 activation in endothelial cells. J Exp Med 211(6):1167–1183. https://doi.org/10.1084/jem.20132330
61. Kanellopoulou T, Alexopoulou A (2013) Bevacizumab in the treatment of hereditary hemorrhagic telangiectasia. Expert Opin Biol Ther 13(9):1315–1323. https://doi.org/10.1517/14712598.2013.813478
62. Ferrara N, Hillan KJ, Novotny W (2005) Bevacizumab (Avastin), a humanized anti-VEGF monoclonal antibody for cancer therapy. Biochem Biophys Res Commun 333(2):328–335. https://doi.org/10.1016/j.bbrc.2005.05.132
63. Bose P, Holter JL, Selby GB (2009) Bevacizumab in hereditary hemorrhagic telangiectasia. N Engl J Med 360(20):2143–2144
64. Dheyauldeen S, Ostertun Geirdal A, Osnes T, Vartdal LS, Dollner R (2012) Bevacizumab in hereditary hemorrhagic telangiectasia-associated epistaxis: effectiveness of an injection protocol based on the vascular anatomy of the nose. Laryngoscope 122(6):1210–1214. https://doi.org/10.1002/lary.23303
65. Walker EJ, Su H, Shen F, Degos V, Amend G, Jun K, Young WL (2012) Bevacizumab attenuates VEGF-induced angiogenesis and vascular malformations in the adult mouse brain. Stroke 43(7):1925–1930. https://doi.org/10.1161/STROKEAHA.111.647982
66. Crist A, Young C, Meadows SM (2017) Characterization of arteriovenous identity in the developing neonate mouse retina. Gene Expr Patterns 23–24:22–31. https://doi.org/10.1016/j.gep.2017.01.002
67. Sobczak M, Dargatz J, Chrzanowska-Wodnicka M (2010) Isolation and culture of pulmonary endothelial cells from neonatal mice. J Vis Exp. https://doi.org/10.3791/2316